ENGINEERING

Isotropic transmission of magnon spin information without a magnetic field

Arabinda Haldar,[1,2] Chang Tian,[2] Adekunle Olusola Adeyeye[2]*

Spin-wave devices (SWD), which use collective excitations of electronic spins as a carrier of information, are rapidly emerging as potential candidates for post-semiconductor non-charge-based technology. Isotropic in-plane propagating coherent spin waves (magnons), which require magnetization to be out of plane, is desirable in an SWD. However, because of lack of availability of low-damping perpendicular magnetic material, a usually well-known in-plane ferrimagnet yttrium iron garnet (YIG) is used with a large out-of-plane bias magnetic field, which tends to hinder the benefits of isotropic spin waves. We experimentally demonstrate an SWD that eliminates the requirement of external magnetic field to obtain perpendicular magnetization in an otherwise in-plane ferromagnet, $Ni_{80}Fe_{20}$ or permalloy (Py), a typical choice for spin-wave microconduits. Perpendicular anisotropy in Py, as established by magnetic hysteresis measurements, was induced by the exchange-coupled Co/Pd multilayer. Isotropic propagation of magnon spin information has been experimentally shown in microconduits with three channels patterned at arbitrary angles.

INTRODUCTION

Wave-like excitations, such as photons (light waves) (*1*), plasmons (plasma oscillations) (*2*), and magnons (spin waves) (*3*), are attractive for applications in future non-charge-based technologies (*3*–*13*). Spin waves, in particular, are interesting because of their small wavelengths and ease of tunability, in addition to their reconfigurable functionality (*14*). A magnetic conduit is one of the building blocks of a spin-wave device (SWD) that transmits information, encoded in the amplitude/phase of the spin waves (*15*). Spin waves with small wave numbers (that is, large wavelengths) and low frequencies are highly anisotropic. Depending on the orientation of the spin-wave wavevector ($\boldsymbol{k}$) with respect to magnetization ($\boldsymbol{M}$) direction, three different categories are defined: two for in-plane magnetized cases, namely, Damon-Eshbach (DE) spin wave, where $\boldsymbol{M} \perp \boldsymbol{k}$, and backward volume (BV) spin wave, where $\boldsymbol{M} \parallel \boldsymbol{k}$; and one for perpendicular magnetization, namely, forward volume (FV) spin waves, where $\boldsymbol{M} \perp \boldsymbol{k}$ (*16*). Usually, DE spin waves are chosen in demonstrations that use lithographically fabricated microconduits due to their large group velocity—resulting in large propagation length, efficient coupling with inductive excitation elements, and suitability for spin-orbit torque-based control (*17*). However, these devices are inefficient for transmitting spin waves in a curved microconduit (*7*, *18*). On the other hand, FV spin waves support spatially isotropic propagation of spin waves, which could enable transmission of information in any arbitrary directions—advantageous for circuit implementation. Recently, a logic operation (*19*) based on isotropic FV spin waves has been found to outperform their in-plane magnetized counterparts (*20*). The demonstration uses yttrium iron garnet (YIG) biased in the out-of-plane direction with an externally applied magnetic field ($H_a \geq 180$ mT) (*19*). In another development, an improved interferometer based on FV spin waves has been shown using YIG with an out-of-plane magnetic field ($H_a \sim 300$ mT) (*21*). The results provide a foundation for realization of multi-input multi-output logic gates based on isotropic spin waves. However, the benefits of FV spin waves are hindered because of the requirement of a large external out-of-plane magnetic field (*19*, *21*, *22*). In addition, large damping of the available out-of-plane magnetized material, such as Co/Pd, Co/Ni, and CoFeB, restricts their application for conduits in an SWD. It leads to the options of using typical in-plane low-damping materials, such as permalloy (Py) (*3*), YIG (*4*), and Heusler alloys (*23*), and external bias magnetic field seems to be unavoidable. Note that exchange-dominated spin waves with large wave numbers and high frequencies also have isotropic propagation characteristics and they can be excited using spin Hall effect (*4*), spin Seebeck effect (*24*), and parametric pumping (*25*). However, here, we demonstrate the isotropic propagation of coherent, low-energy spin waves with small wave numbers and low frequencies.

Here, we design a spin-wave conduit in which thin Py is exchange-coupled to a multilayer of Co/Pd [well known for its perpendicular anisotropy (*26*)], which induces out-of-plane magnetization in an otherwise in-plane magnetized Py conduit. Thus, it eliminates the need of external stand-by power for biasing purposes. Devices are fabricated using top-down microfabrication techniques. Out-of-plane magnetization in Py has been shown by measuring hysteresis loops using the magneto-optical Kerr effect (MOKE) technique. Micro–Brillouin light scattering (micro-BLS) technique has been used to directly probe spin waves in our devices. Isotropic propagation has been shown in a microconduit with multiple channels at arbitrary angles. The advantages of the proposed devices include the use of existing low-damping materials in isotropic mode, ultralow power operation, suitability for device integration, and nonvolatile operation at room temperature.

RESULTS AND DISCUSSION

The schematic of the micro-BLS experiment and sample architecture have been shown in Fig. 1. In the micro-BLS technique, a monochromatic laser is focused down to ~250 nm, and scattered beam is analyzed using a tandem Fabry-Perot (TFP) interferometer (for details of the BLS experiment, see Methods). Spin waves are excited by using a ground-signal-ground (GSG)–type stripe antenna, which is connected to a radio frequency (RF) signal generator. The direction of the RF field (H_{rf}) due to the RF current (I_{rf}) is shown in the enlarged view of Fig. 1A. Three magnetic microconduits, which are typically 2 μm wide and designed from Cr(5)/Cu(10)/Pd(5)/[Co(0.3)/Pd(1.1)]$_6$/Py(5), Cr(5)/Cu(10)/Pd(5)/[Co(0.3)/Pd(1.1)]$_6$ and Cr(5)/Py(5) multilayers (for details of the sample fabrication, see Methods), are shown

[1]Department of Physics, Indian Institute of Technology Hyderabad, Kandi, Sangareddy, Telangana 502285, India. [2]Department of Electrical and Computer Engineering, National University of Singapore, Singapore 117583, Singapore.
*Corresponding author. Email: eleaao@nus.edu.sg

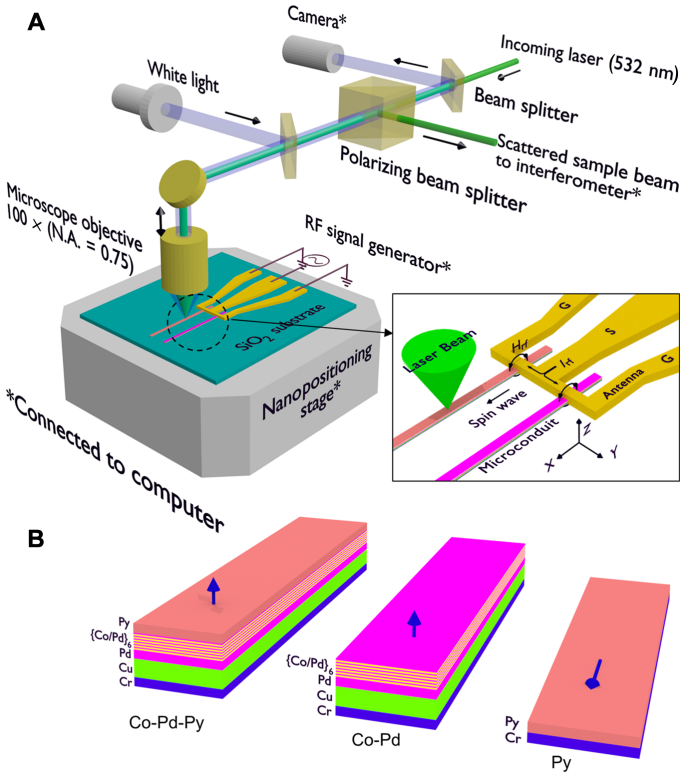

Fig. 1. Experimental configuration and device architecture. (**A**) Schematic of the experimental configuration. A laser beam is focused using a 100× objective onto the sample, which is placed on top of a nanopositioning stage, and the scattered beam is collected by the same objective and directed toward an interferometer by using a polarizing beam splitter. A white light and a camera are collinearly arranged for positioning and stabilization of the sample. Spin waves were excited by a GSG-type stripe antenna, which is shown to be connected to an RF signal generator. The enlarged view of the device shows the direction of the RF current (I_{rf}) and RF field (H_{rf}). Instruments that are controlled by the computer are each marked by an asterisk. N.A., numerical aperture. (**B**) Schematic of the sample cross section showing the Cr(5)/Cu(10)/Pd(5)/$[Co(0.3)/Pd(1.1)]_6$/Py(5) ≡ Co-Pd-Py multilayer structure of the microconduits. The numbers in the first brackets indicate thickness in nm. Two reference microconduits consisting of Cr(5)/Cu(10)/Pd(5)/$[Co(0.3)/Pd(1.1)]_6$ ≡ Co-Pd and Cr(5)/Py(5) ≡ Py are also shown.

in Fig. 1B. Henceforth, they are denoted by Co-Pd-Py, Co-Pd, and Py, respectively. The numbers in the first brackets indicate thickness in nm. Note that Co-Pd and Py microconduits are used as references for comparison with our Co-Pd-Py devices. In the multilayer structures, the bottom-most Cr layer is used for better adhesion. Second-layer Cu is incorporated as a buffer layer, which was found to enhance the coercive field in Co/Pd multilayers (*26*). Third-layer Pd is used as a seed layer to improve the growth of a Co/Pd multilayer. The number of repetitions (here, six) and the thicknesses of the Co and Pd layer for the $[Co(0.3)/Pd(1.1)]_6$ were chosen to achieve large perpendicular anisotropy and sharp magnetization switching (*27*, *28*). Arrows shown Fig. 1B indicate expected remanent magnetization directions.

To investigate the magnetization reversal mechanisms, we have recorded MOKE hysteresis loops in the polar (for Co-Pd-Py and Co-Pd microconduits) and longitudinal (Py microconduit) geometry using a focused laser (635 nm) with a spot diameter of ~5 μm, and the results (squares) are shown in Fig. 2 (A to C). Note that we have fabricated arrays of magnetically isolated microconduits to enhance the MOKE signal. The magnetic hysteresis for the corresponding films (dotted lines) is incorporated for comparison. We have found perpendicular remanent magnetization in Co-Pd-Py with a large coercive field (H_c ~ 118 mT), which is, however, smaller than that of Co-Pd (H_c ~ 240 mT), a widely used multilayer for perpendicular anisotropy. This large difference in the H_c values between Co-Pd-Py and Co-Pd can be attributed to the competition between in-plane magnetic anisotropy of the Py top layer with the perpendicular anisotropy of the Co-Pd bottom layer, which results in a much lower H_c in Co-Pd-Py (*28*). Additionally, we have investigated in-plane MOKE loops for Co-Pd-Py (not shown), and it is similar to a typical hard axis loop. It indicates that the Py top layer—the thickness of which is only 5 nm, comparable to its exchange length—has uniform out-of-plane magnetization due to the exchange-coupled Co/Pd bottom layer. Note that the coercive field does not vary significantly by reducing the width of the Co-Pd-Py microconduit from 2 to 0.5 μm (see fig. S1 for details). We observe in-plane magnetization in Py microconduits, as shown in Fig. 2C. Smaller coercive fields are found in films as compared with the structured microconduits.

We start investigating straight microconduits for spin-wave propagation by recording BLS spectra as a function of RF excitation at remanent magnetization states (H_a = 0). Charge-coupled device (CCD) camera images of the microconduits are shown in Fig. 3 (A to C) in which the bright dots refer to the position of the probing laser spot. Reduction of laser intensity in a Py microconduit appears due to lower reflectivity of the 5-nm-thick Py as compared to the two other thicker microconduits. Before recording the BLS spectra, the devices were initialized with an out-of-plane saturating field and subsequently removed it. The BLS spectra (circles) for Co-Pd-Py, Co-Pd, and Py microconduits in the 3- to 9-GHz frequency range are shown in Fig. 3 (D to F). A noise floor (squares) was measured by turning off the RF excitation. To account for the fluctuations in the BLS intensity, all the spectra are averaged over multiple frequency scans, followed by normalization to the elastic reference peak. It can be seen from Fig. 3D that Co-Pd-Py has prominent spin-wave responses below 6.5 GHz with distinct peaks at 3.3, 4.2, and 5.6 GHz. In contrast, the spectra for two reference samples consisting of Co-Pd (Fig. 3E) and Py (Fig. 3F) microconduits are comparable to the noise floor, which indicate no spin-wave propagation. However, some activity below 4 GHz is observed for the Py microconduit, which has in-plane remanent magnetization (referring to BV mode). To verify this response, we have investigated BLS spectra in the 1.5- to 4-GHz frequency regime for the Py microconduit, and we observe a peak near 1.9 GHz, which corresponds to BV spin waves (see fig. S2 for details). Note that no spin-wave mode is observed above 1.9 GHz for the BV mode. In addition, we have measured DE spin-wave spectra in Co-Pd-Py and compared with Py (see fig. S3 for details). The results show that DE spin waves (fig. S3B) have different spectra than what we see in Fig. 3D. Hence, spin-wave modes observed in Fig. 3D can be associated only with the out-of-plane magnetization of the topmost layer of the Co-Pd-Py conduit. Furthermore, the effect of far-field excitation was found to be insignificant in a control experiment with a broken microconduit (see fig. S4 for details).

To examine the spatial profiles of the three prominent modes at 3.3, 4.2, and 5.6 GHz of Co-Pd-Py, we raster-scanned the sample in steps of 200 nm along the *x* axis and 100 nm along the *y* axis over an area of $3 \times 2\ \mu m^2$. Two-dimensional maps of spin-wave intensity overlaid on top of the scanning electron microscopy (SEM) image of the device are shown in Fig. 3G. Each pixel in Fig. 3G represents the BLS intensity, which is proportional to the spin-wave intensity. Figure 3H shows the spatial decay of the BLS intensity integrated over the transverse section

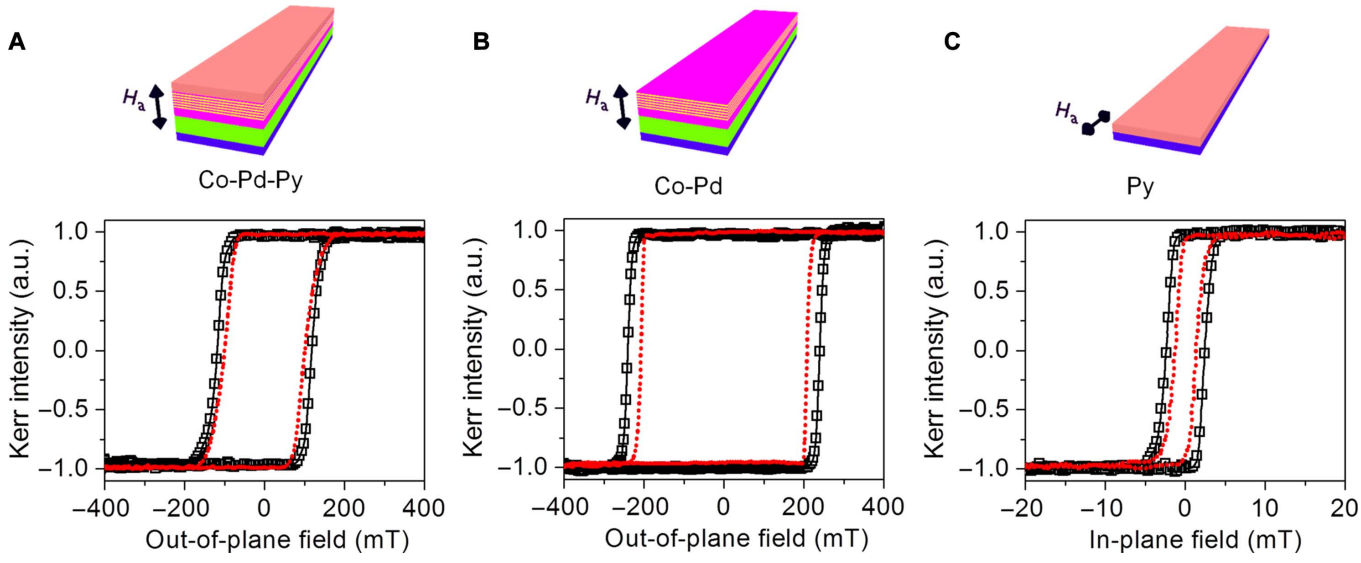

Fig. 2. Device characterization. MOKE hysteresis loops for the microconduits (squares) (**A**) Co-Pd-Py in out-of-plane configuration, (**B**) Co-Pd in out-of-plane configuration, and (**C**) Py in in-plane configuration. a.u., arbitrary units. Direction of the applied field (H_a) are shown by arrows for the three different microconduits. Dotted lines represent the hysteresis loop for a continuous film of the corresponding microconduit.

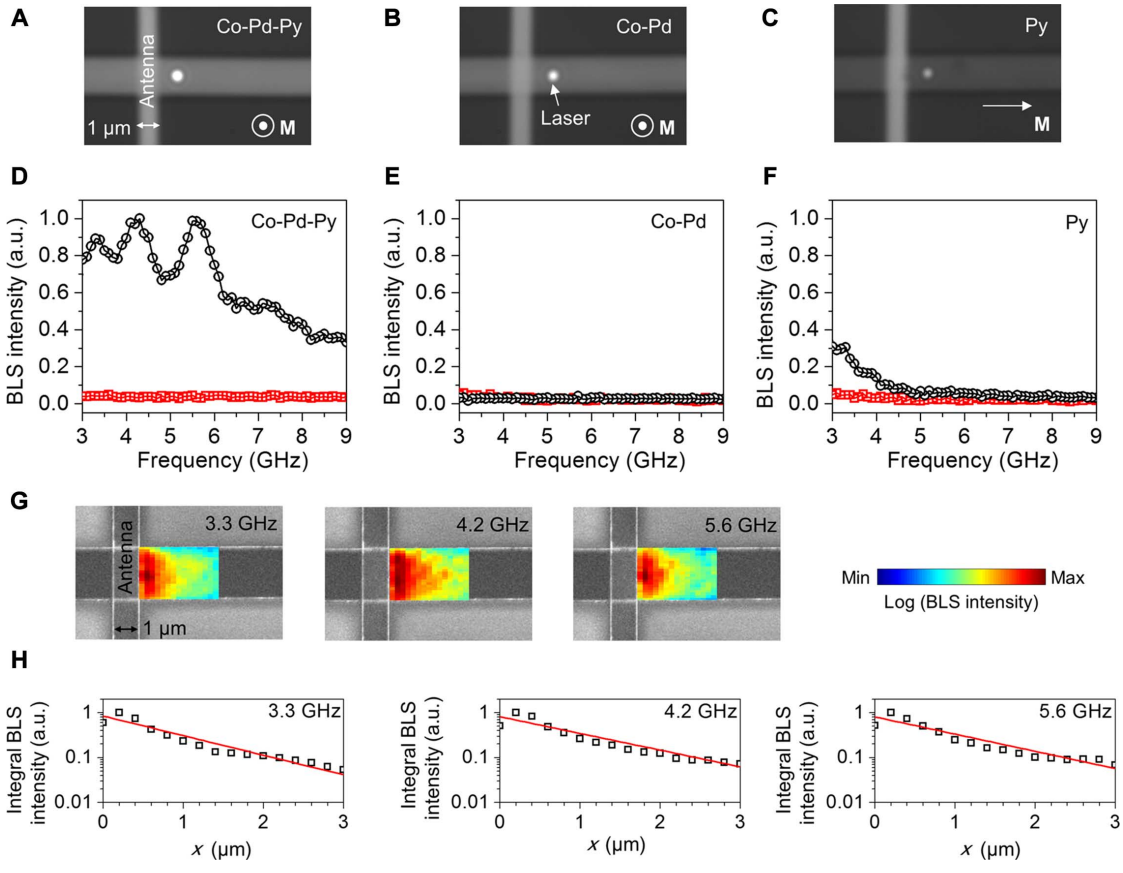

Fig. 3. Spin-wave channeling in straight microconduits. (**A** to **C**) CCD camera images of the three devices, the Co-Pd-Py, Co-Pd, and Py microconduits, showing the laser position where the BLS spectra were recorded. Remanent magnetization directions are indicated by arrows. (**D** to **F**) BLS spectra (circles) as a function of RF for the three devices at remanence. The spectra were compared with the noise floor (squares) obtained without RF excitation. (**G**) Two-dimensional spin-wave intensity maps overlaid on SEM images of the Co-Pd-Py microconduit at 3.3, 4.2, and 5.6 GHz recorded over an area of 3 × 2 μm^2. Each pixel corresponds to BLS intensity at that position. (**H**) Dependence of BLS integral intensity (squares) on the propagation coordinate for the three different modes at 3.3, 4.2, and 5.6 GHz along the center of the Co-Pd-Py microconduit. Lines refer to the fit to the experimental data using an exponential function, as discussed in the text.

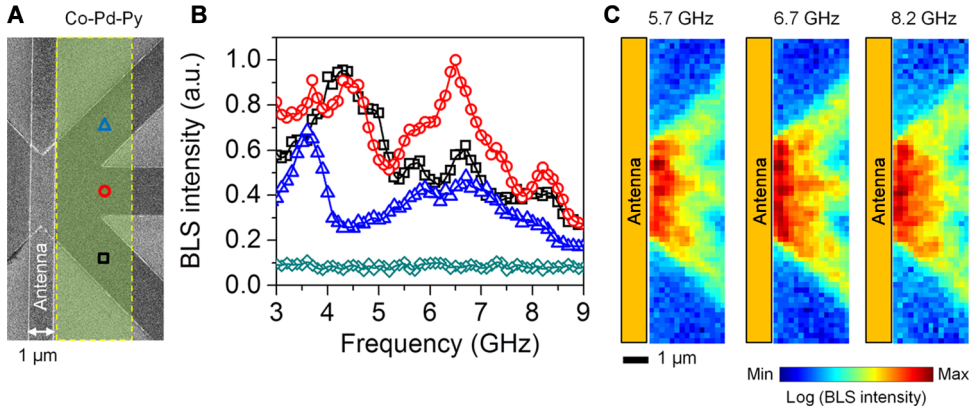

Fig. 4. Isotropic spin-wave flow. (**A**) SEM image of the concept device in which a Co-Pd-Py conduit has three channels at three different angles. Antenna is placed at the three-channel junction. (**B**) BLS spectra as a function RF recorded at three channels indicated by different symbols in the SEM image. (**C**) Two-dimensional spin wave intensity maps at 5.7, 6.7, and 8.2 GHz recorded over an area of 3 × 12 μm^2. Each pixel corresponds to BLS intensity at that position.

(*y* axis) of the two-dimensional intensity maps. Note the logarithmic scale for the BLS integral intensity. Lines are the fit to an exponential function of the form $\exp(-2x/\lambda)$, where λ is the decay length, which is found to be ~2 μm. This value is close to that of surface waves excited by spin-transfer torque (*5*, *29*) and surface waves in magnetic conduits based on microstripes (*30*) and dipolar-coupled nanomagnetic chains (*18*). A systematic investigation of the spin-wave spectra as a function of the width of the Co-Pd-Py microconduits is shown in fig. S5.

Isotropic propagation of information, a cornerstone of an SWD, is demonstrated in a concept Co-Pd-Py microconduit, which consists of three channels at different angles. Figure 4A shows the SEM image of this device where the input was realized with the stripe antenna placed at the three-channel junction and the output was measured optically by using the micro-BLS technique at positions indicated by squares, circles, and triangles. For device integration, our input and output methodologies can be substituted by local electrical techniques, such as spin-transfer torque (*5*, *29*) and spin Hall effect (*4*) for the first, and inverse spin Hall effect (*4*, *31*) for the latter. The recorded BLS spectra as a function of RF excitation frequency and different symbols that correspond to different channels (as shown in Fig. 4A) are shown in Fig. 4B. Noise floor (diamonds) is included for reference. Three common modes can be observed at around 5.7, 6.7, and 8.2 GHz in all the channels. At lower frequencies, top (squares) and central (circles) channels have similar modes. However, one of the modes at 4.2 GHz is absent in the bottom (triangles) channel. It may be attributed to the symmetry of the mode with respect to the excitation process with the stripe antenna. Two-dimensional spatial profiles at 5.7, 6.7, and 8.2 GHz are shown in Fig. 4C, which were obtained by raster-scanning the laser spot over an area of 3 × 12 μm^2 in steps of 200 nm. Observation of similar spectra for three channels, which are at different angles, refers to the isotropic nature of the propagating modes. In contrast, note here that the spin-wave spectra vary with varying the curvature of the microconduit for DE spin waves typically used so far (*18*, *32*).

Finally, we discuss the potential of the isotropic SWDs for on-chip manipulation and long-range propagation for application point of view. Spin-orbit torque (*33*) or Oersted field from dc (*34*) is the potential option for local manipulation of spin waves. On the other hand, using low-damping material, such as Heusler alloys (*23*) and ultrathin YIG films (*35*), or the spin-orbit torque (*36*) could enhance the coherent propagation length of spin waves.

To summarize, we have demonstrated a novel route for realizations of isotropic spin wave–based devices by eliminating the need for an external magnetic field, which had been an elusive goal until now. The design of the magnetic conduit is such that an out-of-plane magnetization is naturally induced in the top Py layer because of perpendicular anisotropy induced by the exchange-coupled Co/Pd bottom layer. Remanent magnetic states are substantiated by polar MOKE hysteresis measurements. Propagation of FV spin waves has been directly probed using the micro-BLS technique, and FV modes are identified unambiguously by carrying out additional measurements in BV and DE geometries. Isotropic propagation of the spin waves is shown by using a microconduit with three channels at arbitrary angles. The results have significant implications in non-charge-based information processing and paves the way for the realization of isotropic spin wave–based devices.

METHODS

Sample fabrication

Devices were fabricated on top of oxidized Si substrates by using a combination of multilevel electron beam lithography and optical lithography techniques. In a first step, the substrate was spin-coated with a positive electron beam resist polymethyl methacrylate, followed by electron beam lithography to pattern the magnetic microconduits. Subsequently, the substrate was developed in a solution of methyl isobutyl ketone and isopropyl alcohol with 1:3 proportion. Multilayer conduit structure consisting of Cr(5)/Cu(10)/Pd(5)/$[Co(0.3)/Pd(1.1)]_6$/Py(5) was deposited using electron beam evaporation (for Cr, Cu, and Py) and sputtering (for Co and Pd) in the same chamber with a base pressure of 2 × 10^{-8} torr without breaking the vacuum. The numbers within the first brackets indicate the thickness of the corresponding material in nm. The number of repetitions is six for the Co/Pd multilayer. The desired microconduits were obtained after metal lift-off in acetone assisted by ultrasonic agitation. In a second step, a 1-μm-wide GSG-type stripe antenna was fabricated using electron beam lithography and lift-off processes, as described above. The antenna is made from Cr(5)/Au(70), where Cr and Au were deposited using electron beam evaporation and sputtering technique, respectively. In a third step, optical lithography technique was used to pattern the larger contact pads of the antenna using PFi positive photoresist and AZ 300 MIF developer. It was followed by the deposition of Cr(5)/Au(200) with a

subsequent lift-off process. The stripe antennae were designed to have 50-ohm impedance. Two reference devices were also fabricated on two separate substrates using the same steps. Magnetic microconduits of these reference samples are made from Cr(5)/Cu(10)/Pd(5)/[Co(0.3)/Pd(1.1)]$_6$ and Cr(5)/Py(5) layers.

BLS spectro-microscopy

BLS is a unique technique for investigation of spin waves that enables measurements in frequency, space, time, and phase domains (*37*, *38*). It is based on inelastic light scattering of incident laser beam from the spin waves of a magnetic medium due to the conservation of total energy and angular momentum. The scattered laser beam from the magnetic sample was analyzed using a TFP interferometer (TFP-1, JRS Scientific Instruments), which operates in six-pass geometry to enhance the weak magnetic signal (inelastic scattering) from a strong elastic background. In a micro-BLS setup, a monochromatic green laser (wavelength, 532 nm; power, 1 mW) was focused down to a diffraction-limited spot diameter of ~250 nm by using a large–numerical aperture 100× objective. A collinear white light and camera arrangement was used to position and view the devices. The devices were placed on top a piezo-controlled nanopositioning stage. The long-term image stabilization with respect to the laser spot was continuously monitored by using a computer-controlled active-feedback algorithm. Two-dimensional spatial profiles of the spin-wave modes were obtained by raster-scanning the sample in steps of 100 or 200 nm using a closed-loop piezo scanner. Spin waves in the devices were excited by using an RF signal generator (0 to 20 GHz) connected to a GSG-type stripe antenna. The width (d = 1 μm) of the antenna defines the upper limit of the wave vector, $k_{max} = 2\pi/d$ = 6.2 rad/μm (*39*).

SUPPLEMENTARY MATERIALS

Supplementary material for this article is available at http://advances.sciencemag.org/cgi/content/full/3/7/e1700638/DC1

fig. S1. Width dependence of magnetic hysteresis in Co-Pd-Py microconduits.
fig. S2. BV spin waves in a Py microconduit.
fig. S3. DE spin waves in Co-Pd-Py and Py microconduits.
fig. S4. Effect of far-field excitation by the antenna.
fig. S5. Width dependence of spin wave spectrum in Co-Pd-Py microconduits.
fig. S6. Anisotropic propagation of spin waves when magnetized in-plane.

REFERENCES AND NOTES

1. D. Brunner, M. C. Soriano, C. R. Mirasso, I. Fischer, Parallel photonic information processing at gigabyte per second data rates using transient states. *Nat. Commun.* **4**, 1364 (2013).
2. A. I. Fernández-Domínguez, F. J. García-Vidal, L. Martín-Moreno, Unrelenting plasmons. *Nat. Photonics* **11**, 8–10 (2017).
3. A. V. Chumak, V. I. Vasyuchka, A. A. Serga, B. Hillebrands, Magnon spintronics. *Nat. Phys.* **11**, 453–461 (2015).
4. L. J. Cornelissen, J. Liu, R. A. Duine, J. B. Youssef, B. J. van Wees, Long-distance transport of magnon spin information in a magnetic insulator at room temperature. *Nat. Phys.* **11**, 1022–1026 (2015).
5. S. Urazhdin, V. E. Demidov, H. Ulrichs, T. Kendziorczyk, T. Kuhn, J. Leuthold, G. Wilde, S. O. Demokritov, Nanomagnonic devices based on the spin-transfer torque. *Nat. Nanotechnol.* **9**, 509–513 (2014).
6. M. Vogel, A. V. Chumak, E. H. Waller, T. Langner, V. I. Vasyuchka, B. Hillebrands, G. von Freymann, Optically reconfigurable magnetic materials. *Nat. Phys.* **11**, 487–491 (2015).
7. K. Vogt, F. Y. Fradin, J. E. Pearson, T. Sebastian, S. D. Bader, B. Hillebrands, A. Hoffmann, H. Schultheiss, Realization of a spin-wave multiplexer. *Nat. Commun.* **5**, 3727 (2014).
8. H. Yu, G. Duerr, R. Huber, M. Bahr, T. Schwarze, F. Brandl, D. Grundler, Omnidirectional spin-wave nanograting coupler. *Nat. Commun.* **4**, 2702 (2013).
9. A. Khitun, M. Bao, K. L. Wang, Magnonic logic circuits. *J. Phys. D Appl. Phys.* **43**, 264005 (2010).
10. R. L. Stamps, S. Breitkreutz, J. Åkerman, A. V. Chumak, Y. C. Otani, G. E. W. Bauer, J.-U. Thiele, M. Bowen, S. A. Majetich, M. Kläui, The 2014 magnetism roadmap. *J. Phys. D Appl. Phys.* **47**, 333001 (2014).
11. K. Wagner, A. Kákay, K. Schultheiss, A. Henschke, T. Sebastian, H. Schultheiss, Magnetic domain walls as reconfigurable spin-wave nanochannels. *Nat. Nanotechnol.* **11**, 432–436 (2016).
12. C. S. Davies, A. Francis, A. V. Sadovnikov, S. V. Chertopalov, M. T. Bryan, S. V. Grishin, D. A. Allwood, Y. P. Sharaevskii, S. A. Nikitov, V. V. Kruglyak, Towards graded-index magnonics: Steering spin waves in magnonic networks. *Phys. Rev. B* **92**, 020408 (2015).
13. V. E. Demidov, S. Urazhdin, S. O. Demokritov, Direct observation and mapping of spin waves emitted by spin-torque nano-oscillators. *Nat. Mater.* **9**, 984–988 (2010).
14. D. Grundler, Reconfigurable magnonics heats up. *Nat. Phys.* **11**, 438–441 (2015).
15. T. Schneider, A. A. Serga, B. Leven, B. Hillebrands, R. L. Stamps, M. P. Kostylev, Realization of spin-wave logic gates. *Appl. Phys. Lett.* **92**, 022505 (2008).
16. B. A. Kalinikos, A. N. Slavin, Theory of dipole-exchange spin wave spectrum for ferromagnetic films with mixed exchange boundary conditions. *J. Phys. C Solid State Phys.* **19**, 7013 (1986).
17. V. E. Demidov, S. O. Demokritov, Magnonic waveguides studied by microfocus brillouin light scattering. *IEEE Trans. Magn.* **51**, 1–15 (2015).
18. A. Haldar, D. Kumar, A. O. Adeyeye, A reconfigurable waveguide for energy-efficient transmission and local manipulation of information in a nanomagnetic device. *Nat. Nanotechnol.* **11**, 437–443 (2016).
19. S. Klingler, P. Pirro, T. Brächer, B. Leven, B. Hillebrands, A. V. Chumak, Spin-wave logic devices based on isotropic forward volume magnetostatic waves. *Appl. Phys. Lett.* **106**, 212406 (2015).
20. S. Klingler, P. Pirro, T. Brächer, B. Leven, B. Hillebrands, A. V. Chumak, Design of a spin-wave majority gate employing mode selection. *Appl. Phys. Lett.* **105**, 152410 (2014).
21. N. Kanazawa, T. Goto, K. Sekiguchi, A. B. Granovsky, C. A. Ross, H. Takagi, Y. Nakamura, M. Inoue, Demonstration of a robust magnonic spin wave interferometer. *Sci. Rep.* **6**, 30268 (2016).
22. A. B. Ustinov, B. A. Kalinikos, E. Lähderanta, Nonlinear phase shifters based on forward volume spin waves. *J. Appl. Phys.* **113**, 113904 (2013).
23. T. Sebastian, Y. Ohdaira, T. Kubota, P. Pirro, T. Brächer, K. Vogt, A. A. Serga, H. Naganuma, M. Oogane, Y. Ando, B. Hillebrands, Low-damping spin-wave propagation in a micro-structured $Co_2Mn_{0.6}Fe_{0.4}Si$ Heusler waveguide. *Appl. Phys. Lett.* **100**, 112402 (2012).
24. B. L. Giles, Z. Yang, J. S. Jamison, R. C. Myers, Long-range pure magnon spin diffusion observed in a nonlocal spin-Seebeck geometry. *Phys. Rev. B* **92**, 224415 (2015).
25. C. W. Sandweg, Y. Kajiwara, A. V. Chumak, A. A. Serga, V. I. Vasyuchka, M. B. Jungfleisch, E. Saitoh, B. Hillebrands, Spin pumping by parametrically excited exchange magnons. *Phys. Rev. Lett.* **106**, 216601 (2011).
26. X. M. Liu, P. Ho, J. S. Chen, A. O. Adeyeye, Magnetization reversal and magnetoresistance behavior of perpendicularly magnetized $[Co/Pd]_4$/Au/$[Co/Pd]_2$ nanowires. *J. Appl. Phys.* **112**, 073902 (2012).
27. S. Pal, B. Rana, O. Hellwig, T. Thomson, A. Barman, Tunable magnonic frequency and damping in $[Co/Pd]_8$ multilayers with variable Co layer thickness. *Appl. Phys. Lett.* **98**, 082501 (2011).
28. T. N. A. Nguyen, V. Fallahi, Q. T. Le, S. Chung, S. M. Mohseni, R. K. Dumas, C. W. Miller, J. Akerman, Investigation of the tunability of the spin configuration inside exchange coupled springs of hard/soft magnets. *IEEE Trans. Magn.* **50**, 1–6 (2014).
29. M. Madami, S. Bonetti, G. Consolo, S. Tacchi, G. Carlotti, G. Gubbiotti, F. B. Mancoff, M. A. Yar, J. Åkerman, Direct observation of a propagating spin wave induced by spin-transfer torque. *Nat. Nanotechnol.* **6**, 635–638 (2011).
30. V. E. Demidov, S. O. Demokritov, K. Rott, P. Krzysteczko, G. Reiss, Self-focusing of spin waves in Permalloy microstripes. *Appl. Phys. Lett.* **91**, 252504 (2007).
31. Y. Kajiwara, K. Harii, S. Takahashi, J. Ohe, K. Uchida, M. Mizuguchi, H. Umezawa, H. Kawai, K. Ando, K. Takanashi, S. Maekawa, E. Saitoh, Transmission of electrical signals by spin-wave interconversion in a magnetic insulator. *Nature* **464**, 262–266 (2010).
32. P. Clausen, K. Vogt, H. Schultheiss, S. Schäfer, B. Obry, G. Wolf, P. Pirro, B. Leven, B. Hillebrands, Mode conversion by symmetry breaking of propagating spin waves. *Appl. Phys. Lett.* **99**, 162505 (2011).
33. D. Bhowmik, L. You, S. Salahuddin, Spin Hall effect clocking of nanomagnetic logic without a magnetic field. *Nat. Nanotechnol.* **9**, 59–63 (2014).
34. S. O. Demokritov, A. A. Serga, A. André, V. E. Demidov, M. P. Kostylev, B. Hillebrands, A. N. Slavin, Tunneling of dipolar spin waves through a region of inhomogeneous magnetic field. *Phys. Rev. Lett.* **93**, 047201 (2004).
35. M. Collet, O. Gladii, M. Evelt, V. Bessonov, L. Soumah, P. Bortolotti, S. O. Demokritov, Y. Henry, V. Cros, M. Bailleul, V. E. Demidov, A. Anane, Spin-wave propagation in ultra-thin YIG based waveguides. *Appl. Phys. Lett.* **110**, 092408 (2017).
36. M. Evelt, V. E. Demidov, V. Bessonov, S. O. Demokritov, J. L. Prieto, M. Muñoz, J. B. Youssef, V. V. Naletov, G. de Loubens, O. Klein, M. Collet, K. Garcia-Hernandez, P. Bortolotti, V. Cros, A. Anane, High-efficiency control of spin-wave propagation in ultra-thin yttrium iron garnet by the spin-orbit torque. *Appl. Phys. Lett.* **108**, 172406 (2016).

37. S. O. Demokritov, V. E. Demidov, Micro-brillouin light scattering spectroscopy of magnetic nanostructures. *IEEE Trans. Magn.* **44**, 6–12 (2008).
38. T. Sebastian, K. Schultheiss, B. Obry, B. Hillebrands, H. Schultheiss, Micro-focused Brillouin light scattering: Imaging spin waves at the nanoscale. *Front. Phys.* **3**, 35 (2015).
39. V. E. Demidov, M. P. Kostylev, K. Rott, P. Krzysteczko, G. Reiss, S. O. Demokritov, Excitation of microwaveguide modes by a stripe antenna. *Appl. Phys. Lett.* **95**, 112509 (2009).

Acknowledgments
Funding: This work was supported by the National Research Foundation, the Prime Minister's Office, Singapore, under its Competitive Research Programme (award no. NRF-CRP10-2012-03). A.O.A. is a member of the Singapore Spintronics Consortium (SG-SPIN). **Author contributions:** A.H. and A.O.A. conceived the project. A.H. carried out the sample fabrication, measurements, and data analysis. C.T. carried out the supporting experiments. A.H. and A.O.A. discussed the results and cowrote the manuscript. **Competing interests:** The authors declare that they have no competing interests. **Data and materials availability:** All data needed to evaluate the conclusions in the paper are present in the paper and/or the Supplementary Materials. Additional data related to this paper may be requested from the authors.

Submitted 3 March 2017
Accepted 12 June 2017
Published 21 July 2017
10.1126/sciadv.1700638

Citation: A. Haldar, C. Tian, A. O. Adeyeye, Isotropic transmission of magnon spin information without a magnetic field. *Sci. Adv.* **3**, e1700638 (2017).

Science Advances

Isotropic transmission of magnon spin information without a magnetic field

Arabinda Haldar, Chang Tian and Adekunle Olusola Adeyeye

Sci Adv **3** (7), e1700638.
DOI: 10.1126/sciadv.1700638